



HAL
open science

Mixed-Valence Conductors from Ni Bis(diselenolene) Complexes with a Thiazoline Backbone

Hadi Hachem, Hengbo Cui, Reizo Kato, Pere Alemany, Enric Canadell,
Olivier Jeannin, Marc Fourmigué, Dominique Lorcy

► **To cite this version:**

Hadi Hachem, Hengbo Cui, Reizo Kato, Pere Alemany, Enric Canadell, et al.. Mixed-Valence Conductors from Ni Bis(diselenolene) Complexes with a Thiazoline Backbone. *Inorganic Chemistry*, 2023, 62, pp.4197. 10.1021/acs.inorgchem.2c04300 . hal-04013829

HAL Id: hal-04013829

<https://hal.science/hal-04013829>

Submitted on 27 Nov 2023

HAL is a multi-disciplinary open access archive for the deposit and dissemination of scientific research documents, whether they are published or not. The documents may come from teaching and research institutions in France or abroad, or from public or private research centers.

L'archive ouverte pluridisciplinaire **HAL**, est destinée au dépôt et à la diffusion de documents scientifiques de niveau recherche, publiés ou non, émanant des établissements d'enseignement et de recherche français ou étrangers, des laboratoires publics ou privés.

Mixed-valence conductors from Ni bis(diselenolene) complexes with a thiazoline backbone

Hadi Hachem,¹ HengBo Cui,² Reizo Kato,³ Pere Alemany,⁴ Enric Canadell,^{5*} Olivier Jeannin,¹ Marc Fourmigué,^{1*} and Dominique Lorcy^{1*}

¹ Institut des Sciences Chimiques de Rennes, Université de Rennes, CNRS, UMR 6226, F-35000 Rennes, France

² (a) Condensed Molecular Materials Laboratory, RIKEN, Wako-shi, Saitama 351-0198, Japan (b) New address: Department of Physics and Astronomy, Institute of Applied Physics, Seoul National University, Seoul 08826, Korea

³ Condensed Molecular Materials Laboratory, RIKEN, Wako-shi, Saitama 351-0198, Japan

⁴ Departament de Ciència de Materials i Química Física and Institut de Química Teòrica i Computacional (IQTCUB), Universitat de Barcelona, Martí i Franquès 1, E-08028 Barcelona, Spain

⁵ Institut de Ciència de Materials de Barcelona, ICMA-B-CSIC, Campus de la UAB, 08193 Bellaterra, Spain

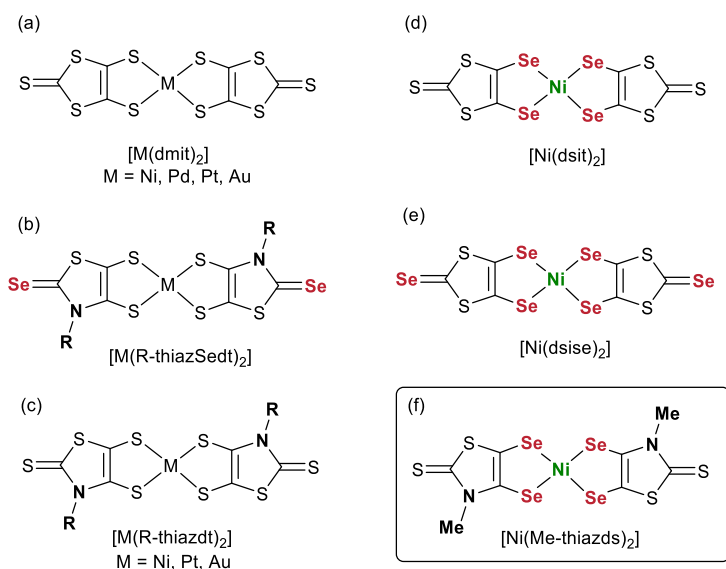
ABSTRACT: Highly conducting, mixed-valence, multi-component nickel bis(*diselenolene*) salts were obtained by electrocrystallization of the monoanionic species $[\text{Ni}(\text{Me-thiazds})_2]^{-1}$ (Me-thiazds: N-methyl-1,3-thiazoline-2-thione-4,5-diselenolate), with 1:2 and 1:3 stoichiometry depending of the counter ion used (Et_4N^+ and $n\text{Bu}_4\text{N}^+$ vs. Ph_4P^+ , respectively). This behavior strongly differs from the corresponding monoanionic *dithiolene* complexes whose oxidation afforded the single component neutral species. This provides additional rare examples of mixed-valence conducting salts of nickel diselenolene complexes, only known in two examples with the dsit (1,3-dithiole-2-thione-4,5-diselenolate) and dsise (1,3-dithiole-2-selone-4,5-diselenolate) ligands. The mixed-valence salts form highly dimerized or trimerized bi- and trimetallic units, rarely seen with such nickel complexes. Transport measurements under high pressure (up to 10 GPa) and band structure calculations confirm the semiconducting character of the $[\text{Ph}_4\text{P}][\text{Ni}(\text{Me-thiazds})_2]_3$ and the *quasi* metallic character of $[\text{Et}_4\text{N}][\text{Ni}(\text{Me-thiazds})_2]_2$ and $[\text{NBu}_4]_x[\text{Ni}(\text{Me-thiazds})_2]_2$ salts ($0 < x < 1$).

■ INTRODUCTION

Nickel and gold bis(dithiolene) complexes have focused a great deal of attention for affording highly conducting systems, either as single-component¹ or as multi-component molecular materials.^{2,3} In order to generate the partially or fully oxidized metal bis(dithiolene) complex, the corresponding monoanionic species $[M(dt)_2]^{-1}$ ($M = Ni, Au$) is generally used in electrocrystallization experiments, and this complex should be at least soluble in a convenient solvent to be oxidized. It should be stressed here that upon electro-oxidation, the large majority of monoanionic gold complexes $[Au(dt)_2]^{-1}$ gives the open-shell species $[Au(dt)_2]^{\bullet,1}$ i.e. the neutral radical complexes, leading to single component molecular conductors, while the monoanionic nickel complexes afford mainly multi-component, mixed-valence conductors (C^+) $[Ni(dt)_2]_n$ ($n = 2,3$) as the prototypical $[Ni(dmit)_2]$ salts (Chart 1a) but rarely the neutral diamagnetic species $[Ni(dt)_2]^0$.

As the chemical approaches to generate the monoanionic Au and Ni complexes are essentially the same, authors generally investigated in parallel both monoanionic metal complexes with the same ligand.^{4,5,6,7,8} Within this frame, we have particularly developed one family of ligands (Chart 1c), namely the N-alkyl-1,3-thiazoline-2-thione-4,5-dithiolate (R-thiazdt, R = alkyl group)⁹ and investigated their corresponding Ni and Au complexes.

Chart 1.



Our chemical approach concerning these complexes relies on the initial preparation of the reduced species such as the d^8 dianionic Ni^{2+} complexes, which are further oxidized in air to the monoanionic open-shell complexes, or for the gold complexes, the direct synthesis of the

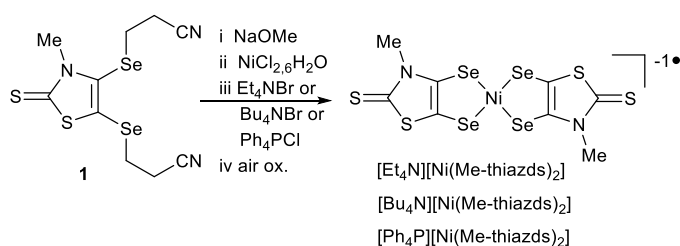
monoanionic d^8 Au^{3+} species. Then through electrochemical oxidation, the neutral species are most often isolated as single component molecular conductors, either with nickel as closed shell species $[Ni(R\text{-thiazdt})_2]^0$ or with gold as radical complexes $[Au(R\text{-thiazdt})_2]^{\bullet}$. Such neutral Ni bis(dithiolene) complexes exhibit, given their closed shell nature, semi conducting behavior for $[Ni(R\text{-thiazdt})]$ ($R = \text{Me, Et, Pr}$).^{10,11} We previously showed, however, that $[Ni(\text{Et-thiazdt})_2]^0$ ($R = \text{Et}$) turns metallic under pressure in the low temperature range when the pressure reaches 4.4 GPa and in the whole temperature range for pressures above 6.9 GPa.¹¹ In the gold series, we have shown that the presence of a substituent smaller than the ethyl one on the ligand allowed us to go from a Mott insulator material for $[Au(\text{Et-thiazdt})_2]^{\bullet}$,¹² to a metallic system for $[Au(\text{Me-thiazdt})_2]^{\bullet}$.¹³ Altogether, the use of the R-thiazdt ligand, either with nickel or gold, systematically led to the neutral complexes, rather than mixed-valence salts, upon electrocrystallization of the monoanionic precursors.

Besides the changes of the R substituent, we also investigated the replacement of sulfur atoms for selenium ones in the metallacycles using the R-thiazds ligand (N-alkyl-1,3-thiazoline-2-thione-4,5-diselenolate) (Chart 1f). Such substitution parallels that reported earlier with the dsit ligand (Chart 1d), the diselenolene analog of dmit. It should be stressed at this point that very few $[M(\text{dsit})_2]$ diselenolene complexes have been reported and structurally characterized to date. They are limited to salts of the monoanionic $[Ni(\text{dsit})_2]^{1-}$ nickel complex,¹⁴ and one single mixed-valence conducting palladium salt, namely $(\text{Me}_4\text{N})[\text{Pd}(\text{dsit})_2]_2$.¹⁵ Besides, one should mention the dsise analogs¹⁶ (Chart 1e) with only one mention of a mixed-valence conducting salt $(\text{Bu}_4\text{N})[Ni(\text{dsise})_2]_2$.¹⁷ We have shown that the oxidation of $[Ni(\text{Et-thiazds})_2]^{1-}$ salts afforded the neutral $[Ni(\text{Et-thiazds})_2]^0$, which exhibits an essentially 1D electronic structure with large band dispersion and small HOMO–LUMO gap and a semi-conducting behavior, with $\sigma_{\text{RT}} = 8 \times 10^{-3} \text{ S cm}^{-1}$ and $E_{\text{act}} = 0.12 \text{ eV}$.¹⁸ By analogy with our recent results on gold diselenolene complexes with the less sterically demanding $R = \text{Me}$ analog $[Au(\text{Me-thiazds})_2]^{1-}$,^{19,20} we investigate here the oxidation of the corresponding monoanionic *N-methyl substituted nickel diselenolene* analogue, which is to say $[Ni(\text{Me-thiazds})_2]^{1-}$ (Chart 1f), in order to see whether this complex during electrocrystallization would generate the unknown single-component conductor $[Ni(\text{Me-thiazds})_2]^0$ or a rare mixed-valence salt. Herein, we describe the synthesis of three monoanionic nickel complexes of the Me-thiazds diselenolene ligand with different counterions, $[C][Ni(\text{Me-thiazds})]$ with $C = \text{Bu}_4\text{N}^+$, Et_4N^+ and Ph_4P^+ and the outcome of their electrocrystallization, providing rare examples of mixed-valence salts of nickel diselenolene complexes, further blessed with high conductivities.

■ RESULTS AND DISCUSSION

Syntheses. The monoanionic nickel diselenolene complexes were prepared starting from the cyanoethyl-protected diselenolene proligand **1** (Scheme 1).⁹ The proligand **1** was deprotected through the addition of sodium methanolate and then, after successive additions of NiCl₂·6H₂O and Ph₄PCl or Et₄NBr or Bu₄NCl, the dianionic species of the nickel complexes were generated. A recrystallization in air from CH₂Cl₂/MeOH (1:4) solution afforded the monoanionic complexes as brown compounds: [Ph₄P][Ni(Me-thiazds)₂], [Et₄N][Ni(Me-thiazds)₂], and [Bu₄N][Ni(Me-thiazds)₂]. Good quality crystals were isolated only for the [Ph₄P][Ni(Me-thiazds)₂] complex.

Scheme 1. Synthetic route toward the monoanionic, radical, Ni bis(diselenolene)complex, [Et₄N][Ni(Me-thiazds)₂], [Bu₄N][Ni(Me-thiazds)₂] and [Ph₄P][Ni(Me-thiazds)₂].



The [Ph₄P][Ni(Me-thiazds)₂] salt crystallizes in the monoclinic system, space group P2₁/n, with both ions in general position. As shown in Figure 1, the diselenolene ligands are disordered on two positions with a 92:8 distribution. Due to the presence of the unsymmetrical Me-thiazds ligand, the *cis* and *trans* isomers can be formed. However, as the Ni complex is localized in a general position in the unit cell, this crystallographic disorder is compatible only with a *trans* configuration of the complex. This disorder is reminiscent to the one observed for the analogous gold complex, [Ph₄P][Au(Me-thiazds)₂].²⁰

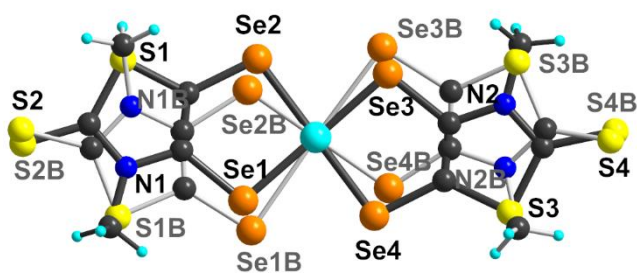


Figure 1. Molecular view of the anion radical species $[\text{Ni}(\text{Me-thiazds})_2]^{-1}$ in $[\text{Ph}_4\text{P}][\text{Ni}(\text{Me-thiazds})_2]$. The two disordered moieties with a 92:8 distribution are highlighted with light grey and black bonds, respectively.

In the solid state, the monoanionic complexes in $[\text{Ph}_4\text{P}][\text{Ni}(\text{Methiazds})]$ interact only along the a axis ($\text{S}\cdots\text{S}$: 3.62 Å), and are well separated by Ph_4P^+ cations associated into inversion-centered pairs in a so-called phenyl embrace motif (Figure S1). The magnetic susceptibility of this complex (Figure S2) is well fitted with a Curie-Weiss law, giving a Curie constant of 0.404, and a θ value of -0.76 K, with a $g = 2.077$ value deduced from EPR experiments.

The redox behavior of the three novel salts has been analyzed by cyclic voltammetry in CH_2Cl_2 using NBU_4PF_6 as supporting electrolyte. Their UV-vis-NIR absorption properties were measured in CH_2Cl_2 at room temperature. For the three salts, the redox system corresponding to the oxidation of the radical anion to the neutral state is not fully reversible, but characterized by a strong adsorption phenomenon occurring at the electrode (Figure 2a). Contrariwise, the redox system corresponding to the reduction into the dianionic species is fully reversible. This trend of deposition of the oxidized species at the electrode upon oxidation is different to the one observed for the N-Et analogues presumably due to a decrease in solubility of the N-Me oxidized species. The counterion does not have a significant influence on the redox potentials (Table 1).

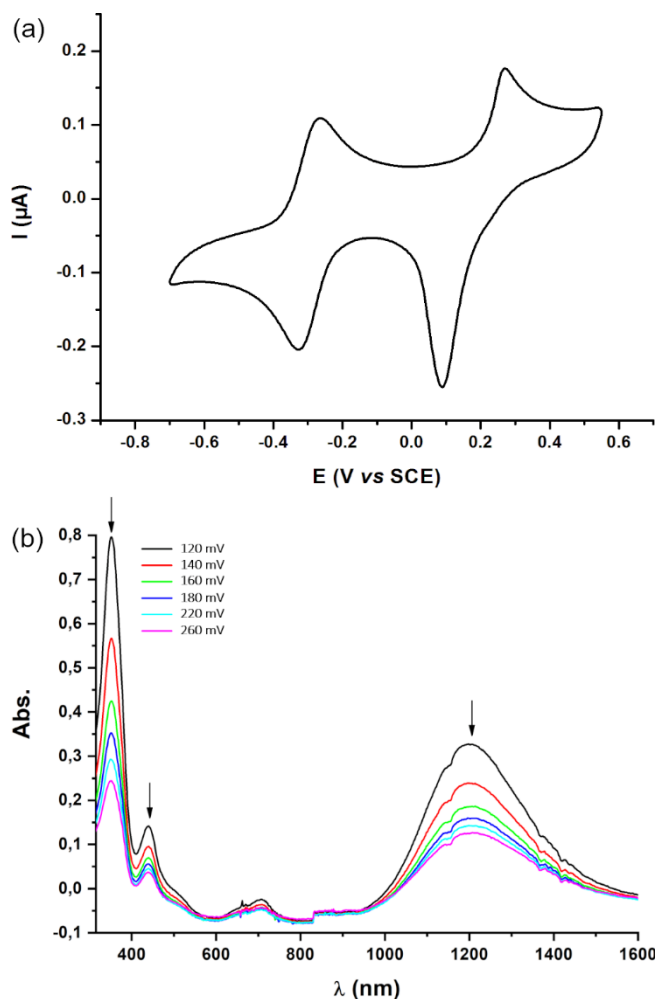


Figure 2. (a) Cyclic voltammetry and (b) UV-vis-NIR monitoring of the electrochemical oxidation of $[\text{PPh}_4][\text{Ni}(\text{Me-thiazds})_2]$ in CH_2Cl_2 , with 0.2M NBu_4PF_6 as a supporting electrolyte.

Table 1. Redox potentials (E in V vs SCE) in CH_2Cl_2 , with 0.1M NBu_4PF_6 as a supporting electrolyte, absorption maxima λ_{max} (nm) and molar extinction coefficients ϵ ($\text{M}^{-1}\text{cm}^{-1}$) for the NIR absorptions of the $[\text{C}][\text{Ni}(\text{Me-thiazds})_2]$ salts ($\text{C} = \text{Ph}_4\text{P}^+, \text{Et}_4\text{N}^+, \text{Bu}_4\text{N}^+$)

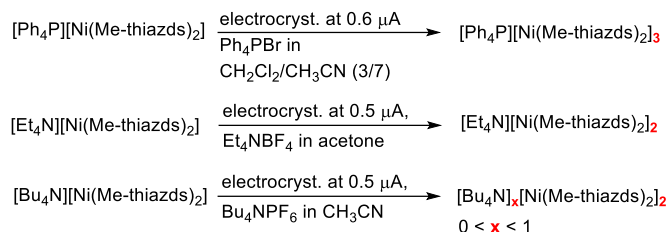
	$E^{-2/-1}$	$E_{\text{pa/pc}}^{-1/0}$	λ_{max} (ϵ) (nm, $\text{M}^{-1}\text{cm}^{-1}$)	Ref
$[\text{Et}_4\text{N}][\text{Ni}(\text{Me-thiazds})_2]^{\text{a}}$	-0.24	+0.21/+0.03	1187 (22300)	9
$[\text{Bu}_4\text{N}][\text{Ni}(\text{Me-thiazds})_2]$	-0.28	+0.24/+0.07	1186 (15800)	this work
$[\text{Ph}_4\text{P}][\text{Ni}(\text{Me-thiazds})_2]$	-0.30	+0.27/+0.09	1184 (16200)	this work

$E = (E_{\text{pa}} + E_{\text{pc}})/2$. ^a in CH_3CN solution. $E_{\text{pa}}/E_{\text{pc}}$: anodic and cathodic peak potentials.

We also performed spectro-electrochemical experiments as they give access to the absorption properties of the neutral species generated at the electrode. The UV-vis-NIR spectroscopic investigations carried out on freshly prepared dichloromethane solution of the monoanionic diselenolene complexes allowed us to determine the absorption maxima (λ_{max}) of the lowest energy NIR electronic transitions for the monoanionic species (Figure 2b). If we compare the spectra obtained for the three monoanionic species, either as a Ph_4P^+ salt, Bu_4N^+ or Et_4N^+ one, there is no influence of the counterion on the wavelength of the low energy absorption band. If we compare now these diselenolene complexes with the dithiolene analogue, $[\text{PPh}_4][\text{Ni}(\text{Me-thiazdt})_2]$ ($\lambda_{\text{max}} = 1278 \text{ nm}$),¹¹ it can be noticed that the replacement of the sulfur atoms by selenium ones induces an hypsochromic shift of this NIR absorption band of about 90 nm. As can be seen in Figure 2b, upon gradual oxidation, an overall decrease of the NIR absorption band was observed resulting from the oxidation of the monoanionic species but concomitantly no spectral signature of the neutral species appeared (Figure 2b). Instead, upon oxidation of the monoanionic species, a strong deposit occurred on the platinum grid, attributed to the formation of the highly insoluble oxidized species.

In order to crystallize and identify the nature of the oxidized species, electrocrystallization experiments were conducted with the three monoanionic complexes. We found that the choice of the electrolyte used in the electrocrystallization cell is particularly important to favor a given phase. Moreover, high quality crystals were obtained only when the counterion of the supporting electrolyte was the same as the counterion of the complex to be oxidized. All electrocrystallizations carried out with these derivatives were reproducible and led systematically to novel multi-component, mixed-valence salts. The salts obtained by electrocrystallization of $[\text{C}][\text{Ni}(\text{Me-thiazds})_2]$ diselenolene complexes (Scheme 2), are of 1:3 stoichiometry, i.e. $[\text{Ph}_4\text{P}][\text{Ni}(\text{Me-thiazds})_2]_3$ starting from the Ph_4P^+ salt, and of 1:2 stoichiometry, i.e. $[\text{Et}_4\text{N}][\text{Ni}(\text{Me-thiazds})_2]_2$ starting with the Et_4N^+ salt, while the stoichiometry is not defined unambiguously in the material obtained from the Bu_4N^+ salt, as the cations could not be clearly identified during the structural refinement (see below). This Bu_4N^+ salt is isostructural with the Et_4N^+ one but the limited increase of the unit cell volume (from 971 \AA^3 to 1016 \AA^3) indicates a sub-stoichiometry in the Bu_4N^+ cation, hence the formulation $[\text{Bu}_4\text{N}]_x[\text{Ni}(\text{Me-thiazds})_2]_2$ with $0 < x < 1$ (See below for details). The obtention of mixed-valence salts comes here in strong contrast with the N-ethyl dithiolene and diselenolene $[\text{Ni}(\text{Et-thiazdt})_2]^0$ and $[\text{Ni}(\text{Et-thiazds})_2]^0$ as well as the N-methyl dithiolene $[\text{Ni}(\text{Me-thiazdt})_2]^0$, all isolated as neutral, single-component species.^{10,11,18}

Scheme 2 Electrocrystallization conditions and outcomes.



Molecular structures. In the three mixed-valence salts, the nickel complexes are organized in the form of highly dimerized, for $[\text{NEt}_4][\text{Ni}(\text{Me-thiazds})_2]_2$ and $[\text{NBu}_4]_x[\text{Ni}(\text{Me-thiazds})_2]_2$, or trimerized motifs for $[\text{PPh}_4][\text{Ni}(\text{Me-thiazds})_2]_3$ (Figure 3). The presence of apical nickel–selenium bonds results in a square pyramidal-like arrangement around the nickel atoms for the dimers, and an octahedral one for the central nickel atom in the trimer. These interactions also shift the structure of the complexes significantly away from planarity, with a strong distortion of the NiSe_2C_2 metallacycles. This type of arrangement has been mostly reported in iron and cobalt bis(dithiolene) complexes, where they are described as M-X dimers or trimers ($\text{X} = \text{S}, \text{Se}$).²¹ For nickel *bis*(dichalcogenolene) complexes, dimers have been reported in $[\text{Ni}(\text{dsit})_2]$ diselenolene salts,^{14,22} and trimers in $\{[\text{Ni}(\text{dddt})_2]_3\}^{2-}$ salts (dddt : 4,5-dihydro-1,4-dithiine-2,3-dithiolate).²³ In the dimers, the two ligands around the Ni1 metal center adopt the *trans* geometry. In the trimer, the *trans* geometry is observed around the central nickel atom (Ni1), while a disorder on two positions is found around Ni2. Refinement of the occupation parameter converged to a $\frac{3}{4} - \frac{1}{4}$ distribution, with the major contribution for the *trans* geometry around Ni2. The intramolecular Ni–Se bonds are shorter than the apical intermolecular (but intradimer) ones by about 0.2 Å. These apical distances are almost identical with those observed in $[\text{Ni}(\text{dsit})_2]$.²² Furthermore, the folding angles of the metallacycles along the Se---Se hinge, $\theta_{\text{Se-Se}}$, are relatively large (6.4–28.1°) reflecting their strong distortion.

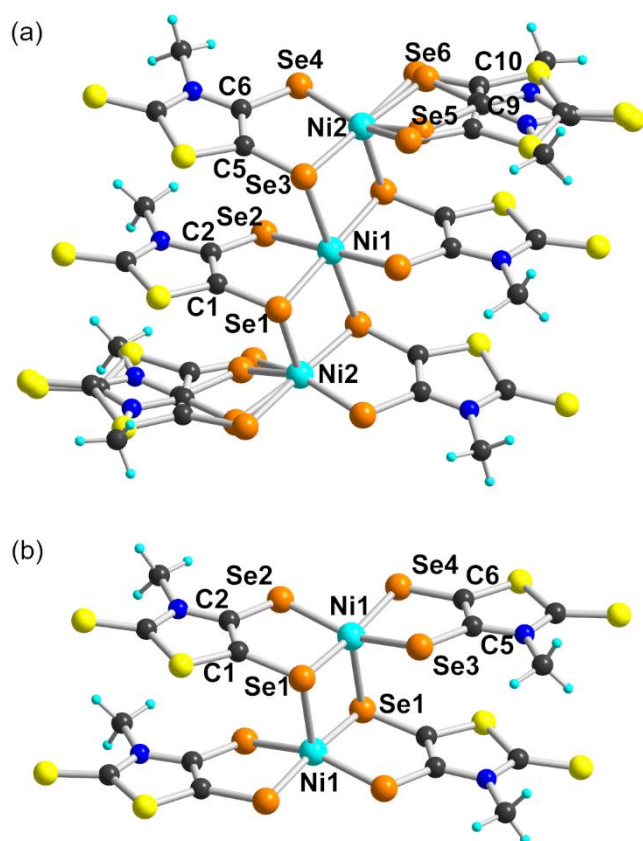


Figure 3. Molecular view of (a) the trimeric motif in $[\text{Ph}_4\text{P}][\text{Ni}(\text{Me-thiazds})_2]_3$ and (b) the dimeric motif in $[\text{Et}_4\text{N}][\text{Ni}(\text{Me-thiazds})_2]_2$.

Table 2. Structural characteristics of the trimeric and dimeric motifs in the mixed-valence salts (θ is the folding angle of the NiSe_2C_2 metallacycle along the $\text{Se}---\text{Se}$ hinge).

$[\text{PPh}_4][\text{Ni}(\text{Me-thiazds})_2]_3$		$[\text{NEt}_4][\text{Ni}(\text{Me-thiazds})_2]_2$		$[\text{NBu}_4]_x[\text{Ni}(\text{Me-thiazds})_2]_2$	
<i>Bond distances (Å)</i>					
Ni1...Ni2	3.4132(11)	Ni1...Ni1	3.1572(10)	Ni1...Ni1	3.1685(14)
Ni1–Se3 apical	2.6371(8)	Ni1–Se1 apical	2.5147(9)	Ni1–Se1 apical	2.5132(13)
Ni2–Se1 apical	2.4591(11)	Ni1–Se1	2.3164(9)	Ni1–Se1	2.3131(12)
Ni1–Se1	2.3913(7)	Ni1–Se2	2.3273(10)	Ni1–Se2	2.3188(14)
Ni1–Se2	2.4109(7)	Ni1–Se3	2.3355(9)	Ni1–Se3	2.3219(13)
Ni2–Se3	2.3290(12)	Ni1–Se4	2.3134(9)	Ni1–Se4	2.3101(13)
Ni2–Se4	2.3529(11)				
Ni2–Se5	2.3447(14)				
Ni2–Se6	2.305(2)				
C1–Se1	1.844(7)	C1–Se1	1.857(6)	C1–Se1	1.844(9)
C2–Se2	1.859(7)	C2–Se2	1.869(6)	C2–Se2	1.845(9)
C5–Se3	1.850(7)	C5–Se3	1.867(6)	C5–Se3	1.881(8)

C6–Se4	1.893(7)	C6–Se4	1.826(6)	C6–Se4	1.846(10)
C9–Se5	1.848(10)				
C10–Se6	1.871(10)				
C1=C2	1.382(10)	C1=C2	1.378(8)	C1=C2	1.365(12)
C5=C6	1.372(10)	C5=C6	1.384(8)	C5=C6	1.335(12)
C9=C10	1.310(12)				
<i>Folding angles (°)</i>					
$\theta_{\text{Se1-Se2}}$	28.1	$\theta_{\text{Se1-Se2}}$	6.7	$\theta_{\text{Se1-Se2}}$	6.4
$\theta_{\text{Se3-Se4}}$	12.9	$\theta_{\text{Se3-Se4}}$	17.3	$\theta_{\text{Se3-Se4}}$	17.0
$\theta_{\text{Se5-Se6}}$	18.0				

Solid state properties. The 1:3 salt with the Ph_4P^+ cation, $[\text{PPh}_4][\text{Ni}(\text{Me-thiazds})_2]_3$, crystallizes in the monoclinic system, space group $C2/c$. The $\text{Ni}(\text{Me-thiazds})_2$ complexes form trimers which are associated into layers in the bc plane alternating along the a axis with layers of Ph_4P^+ cations (Figure 4). The trimerized units pack in a perpendicular fashion, similar to a κ -type phase arrangement. The central nickel atom of the trimer resides on an inversion center, and the phosphorous atom on a twofold axis.

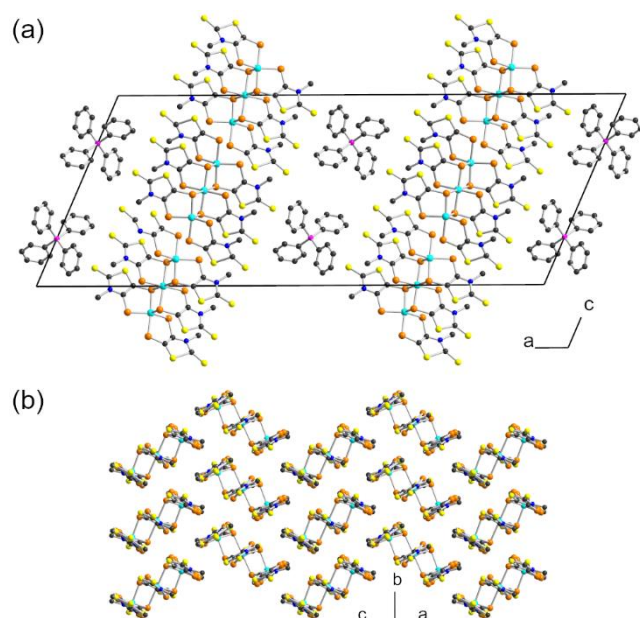


Figure 4. (a) Projection of the unit cell of $[\text{Ph}_4\text{P}][\text{Ni}(\text{Me-thiazds})_2]_3$ along b , (b) detail of the anionic layer showing interactions between trimers in the (bc) plane.

Each trimer interacts with six neighboring trimers in the (bc) plane and the shortest inter-trimer $\text{Se}\cdots\text{Se}$ contacts are found at 3.67 Å, i.e. 94% on the van der Waals contact distance.

The highest occupied and lowest unoccupied levels of one trimer are a set of six levels built from the HOMO and LUMO of the Ni(Me-thiazds)₂ monomers and delocalized within the trimer. Three of these levels are doubly filled in the neutral species. Since the unit cell of the layer contains two trimers, the band structure contains six pairs of bands (Figure 5). These bands exhibit a quite poor energy dispersion, especially those marked with a red arrow, which are those half-filled by the transferred electrons. Such band structure clearly shows that the trimers interact only weakly, thus suggesting this salt to behave as a Mott insulator with one localized (but delocalized within the trimer) $S = \frac{1}{2}$ radical per trimer.

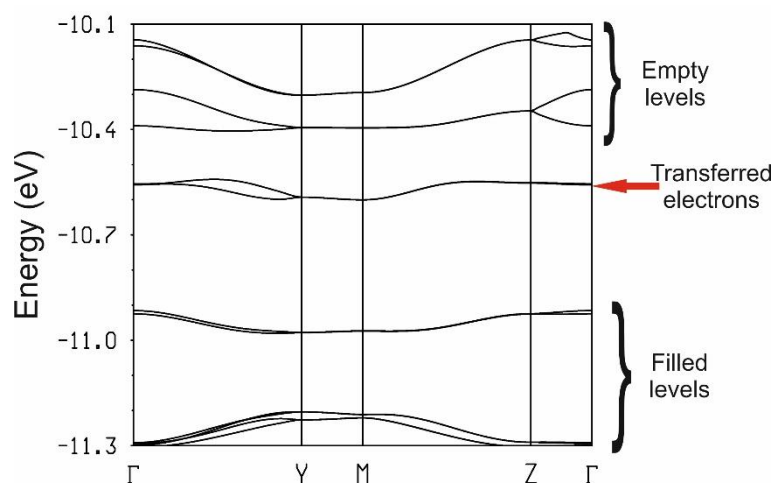


Figure 5. Calculated extended Hückel band structure for the anionic layer of [PPh₄][Ni(Me-thiazds)₂]₃ where $\Gamma = (0, 0)$, $Y = (b^*/2, 0)$, $Z = (0, c^*/2)$, $M = (b^*/2, c^*/2)$. The red arrow points out the bands that would be occupied by the two transferred electrons.

Transport and magnetic measurements confirmed these assumptions. The material shows a semiconducting behavior, with a room temperature conductivity of $4 \times 10^{-4} \text{ S.cm}^{-1}$, and an activation energy of 203 meV (Figure 6). This semiconducting behavior persists at higher pressures (up to 11.9 GPa), with an increase of the RT conductivity by 3 orders of magnitude ($\sigma_{\text{RT}} = 0.25 \text{ S.cm}^{-1}$), while the activation energy is divided by two down to 68 meV at 11.9 GPa. This electronic localization is also confirmed by the temperature dependence of the magnetic susceptibility (Figure S3). It shows a behavior that is well fitted to a Curie-Weiss law, giving a Curie constant of 0.409, and a θ value of +0.92 K. The calculated g value amounts to 2.088, which is very close to what was observed for the monoanionic precursor [PPh₄][Ni(Me-thiazds)₂] ($g = 2.077$). This shows that, due to the strong trimerization, each unit acts as a single radical moiety, with very weak interactions between the $S = \frac{1}{2}$ trimeric species.

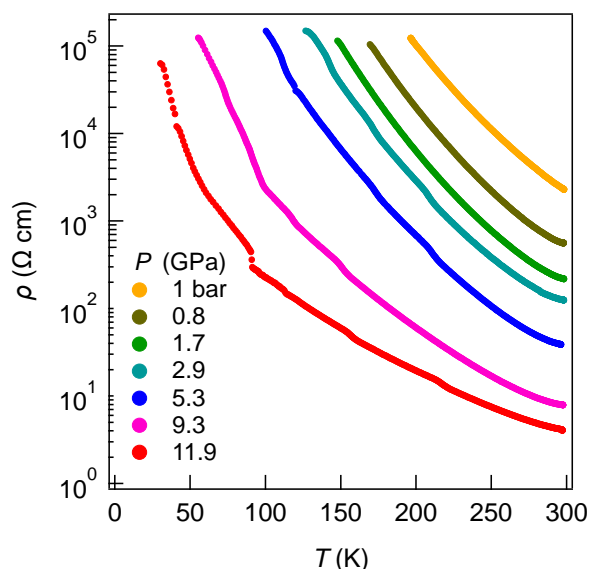


Figure 6. (a) Temperature dependence of the resistivity of $[\text{PPh}_4][\text{Ni}(\text{Me-thiazds})_2]_3$ at different pressures between 1 bar and 11.9 GPa.

The mixed-valence Et_4N^+ salt, $[\text{Et}_4\text{N}][\text{Ni}(\text{Me-thiazds})_2]_2$, crystallizes in the triclinic system, space group $P\bar{1}$, in a 1:2 stoichiometry. The complexes form inversion-centered dimerized units making stacks and the Et_4N^+ cation is disordered on an inversion center. The monoanionic radical dimers and cations form layers in the ab plane that alternate along the c axis (Figure 7).

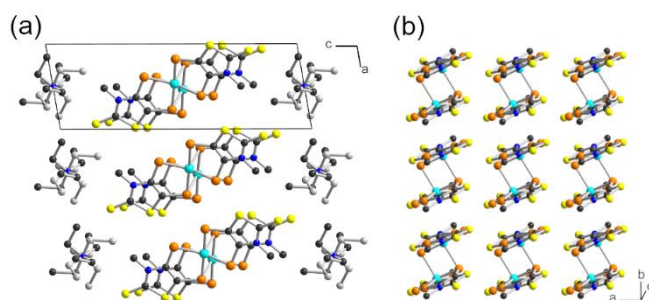


Figure 7 (a) Projection view of the unit cell of $[\text{NEt}_4][\text{Ni}(\text{Me-thiazds})_2]_2$ along b showing in light and dark grey atoms the disorder model on the Et_4N^+ cation, (b) End-on view of the anionic layer. Hydrogen atoms have been omitted for clarity.

The evolution of the conductivity of $[\text{Et}_4\text{N}][\text{Ni}(\text{Me-thiazds})_2]_2$ at ambient pressure shows a semiconducting behavior with a high room temperature conductivity of $6 \text{ S}\cdot\text{cm}^{-1}$ and a very small activation energy of 12 meV. Repeated attempts to measure the conductivity at

higher pressures in the Diamond Anvil Cell (DAC) were unsuccessful as the gold contacts crystals appear to react with the crystals.

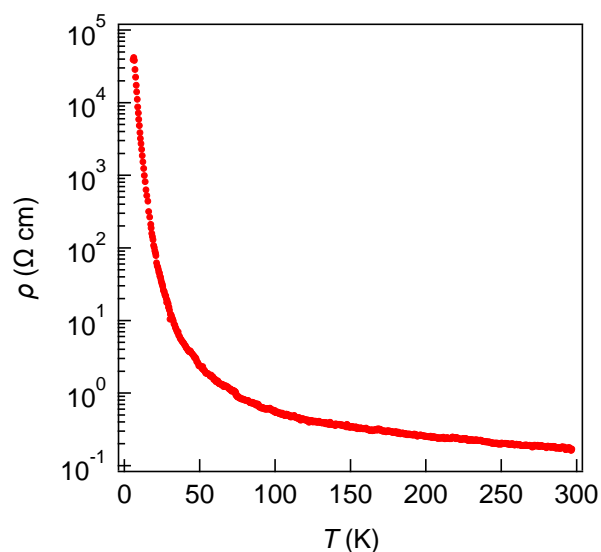


Figure 8. Temperature dependence of the resistivity of $[\text{NEt}_4][\text{Ni}(\text{Me-thiazds})_2]_2$ at ambient pressure

Short inter-dimer $\text{Se}\cdots\text{Se}$ contacts are found along the stacking b axis (down to 3.46 \AA), and between the stacks (down to 3.39 \AA), associated with three types of inter-dimer interactions within the layers, running along b , between neighboring dimers along a , and diagonally along $(a-b)$. The occurrence of these very short $\text{Se}\cdots\text{Se}$ contacts seems to be in conflict with the activated character of the conductivity, suggesting indeed a metallic character. Extended Hückel band structure calculations (Figure S4) as those used above for the 1:3 Ph_4P^+ salt in Figure 5 show that the Fermi level indeed cuts a band with a substantial energy dispersion of $\sim 0.4 \text{ eV}$. Such a dispersion (calculated with the same computational settings)^{2b,24} for this type of dimerized metal bis(dithiolene) type layers is usually associated with a metallic behavior, thus confirming our initial expectation. At this point we decided to turn to DFT calculations that by considering electronic interactions explicitly will allow a more in-depth exploration of this apparent contradiction. The calculated band structure for $[\text{NEt}_4][\text{Ni}(\text{Me-thiazds})_2]_2$ assuming double occupation of the levels is reported in Figure 9a. Because of the strong cation disorder, we removed the cations from the calculation replacing them by a uniform background charge keeping the neutrality of the unit cell. This procedure has been tested in numerous cases and shown to provide band structures almost undistinguishable from those using the full unit cell.^{25,26,27} Because of the very short intra-dimer $\text{Se}\cdots\text{Se}$ contacts and the Ni-over-Se type dimerization (see Figure 3b), the splitting of the HOMO and LUMO levels in a dimeric unit is

not the typical one found in many metal bis(dithiolene) dimerized salts (see Figure 9b).^{2b,3b,27} The bonding/antibonding combinations of the HOMOs are the main components of the lower/upper levels of the set of four dimer orbitals; the bonding/antibonding combinations of the LUMOs occur in between them. Such ordering is essentially kept in the layer according to the band structure of Figure 9a which corresponds to a metallic system. The bonding combinations of both the HOMO and LUMO levels are filled providing a strong stability to the dimers and the electron transferred from the cation partially fills the antibonding combination of the LUMOs. This level ordering is unexpected since in the absence of any calculation and with one electron transferred to the dimer, one would expect that the bonding combination of the LUMOs would house the electron. This level ordering is still another consequence of the so called two-band behavior.^{2b,24,27}

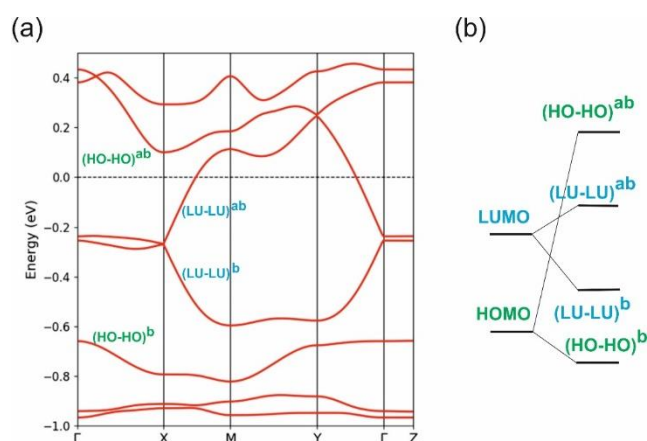


Figure 9. (a) Calculated DFT band structure for $[\text{NEt}_4][\text{Ni}(\text{Me-thiazds})_2]_2$ assuming that all levels are doubly filled. The Fermi level is represented by a dashed line and Γ , X, Y, M, and Z refer to $\Gamma = (0, 0, 0)$, $X = (1/2, 0, 0)$, $Y = (0, 1/2, 0)$, $M = (1/2, 1/2, 0)$ and $Z = (0, 0, 1/2)$ in units of the triclinic Brillouin zone. (b) Schematic diagram showing the splitting of the $\text{Ni}(\text{Me-thiazds})_2$ HOMO and LUMO levels in the $[\text{Ni}(\text{Me-thiazds})_2]_2$ dimers of Figure 3b. The “b” and “ab” labels refer to bonding and antibonding combinations, respectively.

In order to find a plausible explanation for the observed activated conductivity of this salt we carried out spin-polarized DFT calculations to see if states with electrons localized on the dimers more stable than the metallic one could be found. This proved to be a difficult task since our trials invariably converged to the delocalized metallic state. After several unsuccessful attempts, we considered the possibility of some inadequacy in our computational approach, either because of the use of the uniform background charge or from some deficiency in the computational settings that was exaggerating the $\text{Se}\cdots\text{Se}$ interactions, thus favoring the metallic

state. In order to test the latter we carried out calculations with exactly the same computational details for a single-molecule conductor based on a very similar complex, $[\text{Au}(\text{Et-thiazds})_2]$.¹⁹ We were able to reproduce the subtle energy difference between metallic and antiferromagnetic localized states of the previous calculations carried out with a different plane wave based computational approach,¹⁹ so that the problems found for the present case seem not to arise from an inadequate choice of our computational method.

As mentioned above, the use of a uniform background of charge for molecular conductors where counterions exhibit disorder has been tested in numerous cases, and shown to provide band structures almost undistinguishable from those using the full unit cell with the disordered counterion frozen in the majority position.^{25,26,28} Thus, we suspected that the difficulty in converging toward localized states was most likely unrelated to technical problems with the computations. For this reason, we devised a different strategy to search for possible localized states by rigidly shifting the dimers along different directions of the lattice so as to decrease the Se•••Se interactions selectively. As shown in the band structure of Figure 9a, the band widths along the chain direction (Γ -Y) are substantially larger than those along the interchain direction (Γ -X), specially for the partially filled band. Thus, we decided to explore the behavior of a single chain of dimers along the b axis. We used a $2a \times 2b \times 2c$ cell so as to have well separated chains. We found that an antiferromagnetic (AF) state lying very slightly below the metallic state (4 meV/dimer) can be obtained (Figure S5). The ferromagnetic state is considerably higher in energy than the metallic state (40 meV/dimer). The stability of this AF state increases when the dimers are rigidly shifted along the chain, decreasing the Se•••Se contacts between them. However, as soon as the inter-chain interactions are switched on, only the metallic state can be obtained. It is thus clear that the chain of dimers has two almost degenerate states: metallic and AF. The two states are so close in energy that even if the inter-chain interactions are weak, they slightly stabilize the metallic state which becomes the more stable alternative when the total spin is $S = 0$. However, we suspected that if we allowed antiferromagnetic interactions along the inter-chain direction maybe the localized AF state would be the more stable state for the layer, as it was for the isolated chain. A calculation using a $2a \times 2b \times 1c$ cell confirmed this expectation and the fully AF state could be located and was found to be 1 meV/dimer more stable than the metallic state. Of course, this very small energy difference should not be taken at its right face and the only meaningful conclusion of this computational exercise is that $[\text{Et}_4\text{N}][\text{Ni}(\text{Me-thiazds})_2]_2$ has two possible ground states, metallic and localized, which are very close in energy. Why then the present system, although quite conductive as suggested by the calculations, chooses to exhibit a semiconducting

behavior? The simplest possibility would rely on a slight predominance of electronic repulsions over delocalization effects. In that case, a very small pressurization should stabilize the metallic state albeit we were not able to verify it experimentally. However, a plausible answer can be attained after consideration of the results for the Bu_4N^+ salt.

The mixed-valence salt with the Bu_4N^+ cation crystallizes in the triclinic system, space group $P\bar{1}$. The overall structure and organization are very close to that of the Et_4N^+ salt, with strong dimerization of the complex units. For instance, the shorter inter-dimer $\text{Se}\cdots\text{Se}$ contacts along the stacking b axis are now 3.44 Å and those between the stacks now go down to 3.37 Å. These values are very similar to those quoted above for the Et_4N^+ salt, at 3.46 and 3.39 Å respectively. As mentioned above, the strong disorder of the Bu_4N^+ moiety in the crystal structure could not be solved, even when the data collection was performed at low temperatures (150 K). For this reason, the cation was squeezed out of the crystal structure. This issue poses a hurdle in assessing the true stoichiometry between the complexes and cations, a crucial aspect concerning the overall band filling of this salt. Considering the unit cell volume of the Et_4N^+ salt (971 Å³ for 47 non-hydrogen atoms), the Bu_4N^+ salt with 55 non-hydrogen atoms should have, with a 1:2 stoichiometry, a cell volume around 1133 Å³, instead of the observed 1016 Å³ volume. This corresponds to a $[\text{Bu}_4\text{N}]_x[\text{Ni}(\text{Me-thiazds})_2]_2$ salt with an x value of 0.66. Analysis of the SQUEEZE procedure during the structural refinement of $[\text{Bu}_4\text{N}]_x[\text{Ni}(\text{Me-thiazds})_2]_2$ to represent the disordered Bu_4N^+ cation gives a very similar value ($x = 0.70$). As expected from the structural discussion, the calculated DFT band structure is practically identical to that of the Et_4N^+ salt (Figure S6) and the only noticeable effect of the partial occupation of the cation sites is a displacement of the corresponding Fermi level.

The temperature dependence of the resistivity at ambient pressure shows a highly conducting but activated behavior, with $\sigma_{\text{RT}} = 1.25 \text{ S cm}^{-1}$ and $E_{\text{act}} = 19 \text{ meV}$, comparable to those found in the stoichiometric Et_4N^+ salt. Resistivity measurements under pressure could be performed and showed an increase in conductivity and a decrease in activation energy between 1 bar and 4.7 GPa (Figure 10). Further increase in pressure up to 9.6 GPa showed an essentially

semi-metallic behavior over the whole temperature range, with a $\sigma_{RT} = 16 \text{ S cm}^{-1}$ and an activation energy divided by two down to 9 meV.

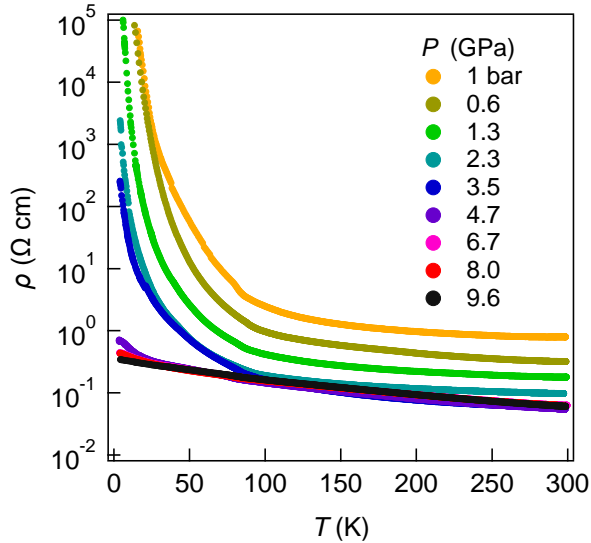


Figure 10. Temperature dependence of resistivity of $[\text{NBu}_4]_x[\text{Ni}(\text{Me-thiazds})_2]_2$ at different pressures.

With these results in mind, we can understand the origin of the activated conductivity of the two salts. The energy difference between the localized and metallic states of the NEt_4^+ salt is extremely small. Because of the non-stoichiometry, the filling of the $(\text{LU-LU})^{\text{ab}}$ bands in $[\text{NBu}_4]_x[\text{Ni}(\text{Me-thiazds})_2]_2$ decreases thus going out of the half-filled situation which is known to favor the localization. Thus, a better conductivity or even a metallic behavior is expected for the NBu_4^+ salt. A simple chemical argument illustrates this point. The activated conductivity of a localized system essentially arises from the electronic repulsion (U) created when an electron jumps from one site (dimer) to the next one. When $x \approx 2/3$, around one third of the dimers do not have any electron in the $(\text{LU-LU})^{\text{ab}}$ level. Consequently, when one electron jumps to one of these empty levels, no electron repulsion is created and the jump is not associated with a strong energy penalty (activation energy). Whereas all jumps are activated in the NEt_4^+ salt, a substantial number of them are non-activated in the NBu_4^+ salt. So to speak, the non-stoichiometry should introduce a kind of metallicity in the system resulting with a much better conductivity than for the NEt_4^+ salt. However, our conductivity measurements do not agree with such expectation. Only under a substantial pressurization a semimetallic state is reached.

There are two basic mechanisms for the occurrence of an electron localization in layers such as those found in the present salts. First, an intrinsic mechanism where the electronic

repulsions drive the localization of electrons (Mott-type mechanism).²⁹ Second, an extrinsic disorder induced localization (Anderson-type mechanism).^{30,31} Although both mechanisms must be simultaneously operative in these salts, the severe disorder in the cation sites and the absence of a clear preference for a localized state in the DFT calculations strongly advocate for the dominance of the cation disorder as the more plausible origin for the activated nature of the conductivity. We believe that the two salts would be metallic in agreement with the occurrence of very short inter-dimer Se...Se contacts if it were not for the severe cationic disorder.

■ CONCLUSIONS

In contrast with nickel bis(R-thiazdt) dithiolene complexes, which afford single-component neutral species, nickel bis(Me-thiazds) diselenolene complexes lead to rare multi-component, mixed-valence salts. Depending on the cation, salts with different stoichiometries were obtained. The PPh_4^+ salt contains anionic layers with trimeric units associated through apical Ni–Se bonds leaving the central nickel atom in an octahedral coordination; it exhibits semiconducting behavior with an activation energy E_{act} of 203 meV. This activated conductivity is kept under pressures up to ~12 GPa although the conductivity increases by three orders of magnitude and E_{act} decreases to 68 meV. The Et_4N^+ and Bu_4N^+ salts contain strongly dimerized units with two intra-dimer Ni–Se bonds leading to a square-pyramidal nickel coordination. The cations in both salts are disordered and the stoichiometry is 1:2 for the Et_4N^+ and 2/3:2 for the Bu_4N^+ salts. The Et_4N^+ compound exhibits a semiconducting behavior at ambient pressure, with a high conductivity ($\sigma_{\text{RT}} = 6 \text{ S cm}^{-1}$) and very low E_{act} (12 meV). Based on a DFT study we suggest that the activated conductivity is mostly disorder-induced. The essentially isostructural NBu_4^+ salt $[\text{NBu}_4]_x[\text{Ni}(\text{Me-thiazds})_2]_2$ is characterized by a non-integer stoichiometry ($x \approx 2/3$) and exhibits a similar semi-conducting behavior, while turning semi-metallic under pressure. At variance with most other systems incorporating these R-thiazdt and R-thiazds ligands which provide the single-component neutral complexes, we demonstrate here that nickel complexes of the Me-thiazds diselenolene ligand are able to organize into highly conducting 2:1 mixed-valence systems with strongly dimerized complexes stabilized by short Ni•••Se intra-dimer bonds. This structural motif contrasts with the well-known $[\text{Pd}(\text{dmit})_2]$ 2:1 salts which exhibit a variety of ground states depending on the choice of cation,³² where the dimeric moieties are associated through metal-metal Pd–Pd intradimer bonds. The observed sensitivity to pressure effects lets us infer that chemical pressure could also be used here to tune their properties, by replacing for example the Et_4N^+ cation by smaller (Me_4N^+ ; Me_4P^+ , Et_3MeN^+ , Et_3MeP^+) or larger ones (Et_4P^+ , Et_4As^+), as exemplified in the $[\text{Pd}(\text{dmit})_2]$ series.³²

■ EXPERIMENTAL SECTION

General. Chemicals and materials from commercial sources were used without further purification. All the reactions were performed under an argon atmosphere. Melting points were measured on a Kofler hot-stage apparatus and are uncorrected. Mass spectra were recorded by the CRMPO, Rennes. Methanol, acetonitrile and dichloromethane were dried using an Inert pure solvent column device. CVs were carried out on a 10^{-3} M solution of complex in CH_2Cl_2 with NBu_4PF_6 0.1 M. Potentials were measured *versus* Saturated Calomel Electrode (SCE). The spectro-electrochemical setup was performed in CH_2Cl_2 with Bu_4NPF_6 0.2 M using a Pt grid as the working electrode, a Pt wire as the counter electrode and SCE reference electrode. A Shimadzu 3600 spectrophotometer was employed to record the UV-vis-NIR spectra. Proligand **1** and $[\text{NEt}_4][\text{Ni}(\text{Me-thiazds})_2]$ were prepared as previously reported.⁹

Syntheses. $[\text{C}][\text{Ni}(\text{Me-thiazds})_2]$. Under inert atmosphere, a solution of sodium methanolate in MeOH (1.5 mmol, prepared from 35 mg of Na in 10 mL of dry MeOH) was added to the proligand **1** (200 mg, 0.5 mmol). After complete dissolution, the solution was stirred at room temperature for 30 mn. Then a solution of $\text{NiCl}_2 \cdot 6\text{H}_2\text{O}$ in MeOH (5 mL) was added, followed 6 hours later by the addition of C^+Br^- (0.5 mmol, 210 mg of PPh_4Br and 161 mg of NBu_4Br). After stirring for 15 h, the formed precipitate was filtered and recrystallized under an air atmosphere from $\text{CH}_2\text{Cl}_2/\text{MeOH}$ 20/80 to afford the monoanion complex as dark crystals.

$[\text{PPh}_4][\text{Ni}(\text{Me-thiazds})_2]$, $\text{C}_{32}\text{H}_{26}\text{N}_2\text{NiPS}_4\text{Se}_4$, brown yellow crystals; Yield: 59% (143 mg); Mp = 178°C ; HRMS (ESI) Calcd. for $[\text{C}_8\text{H}_6\text{N}_2\text{S}_4^{58}\text{Ni}^{80}\text{Se}_4]^-$: 635.54336 Found: 635.5434; Anal. calcd. for $\text{C}_{32}\text{H}_{26}\text{N}_2\text{NiPS}_4\text{Se}_4$: C, 39.53; H, 2.70; N, 2.88; S, 13.19. Found: C, 39.53; H, 2.77; N, 3.02; S, 13.54

$[\text{NBu}_4][\text{Ni}(\text{Me-thiazds})_2]$, $\text{C}_{24}\text{H}_{42}\text{N}_3\text{NiS}_4\text{Se}_4$, brown yellow crystals; Yield: 32% (70 mg); Mp = 190°C ; HRMS (ESI) Calcd. for $[\text{C}_8\text{H}_6\text{N}_2\text{S}_4^{58}\text{Ni}^{80}\text{Se}_4]^-$: 635.54336 Found: 635.5425; Anal. calcd. for $[\text{C}_{24}\text{H}_{42}\text{N}_3\text{NiS}_4\text{Se}_4 \cdot \text{CH}_2\text{Cl}_2]$: C, 31.27; H, 4.62; N, 4.38. Found: C, 31.51; H, 4.75; N, 4.51.

Electrocrystallizations. They were systematically performed in two-compartment cells with Pt electrodes under inert atmosphere with degassed solvents.

$[PPh_4][Ni(Me-thiazds)_2]_3$. A solution of PPh_4Br (200 mg) dissolved in 10 mL of CH_2Cl_2/CH_3CN (3/7) was introduced in both compartments as supporting electrolyte. The nickel complex $[PPh_4][Ni(Me-thiazds)_2]$ (10 mg) was introduced in the anodic compartment. The current intensity was adjusted to 0.6 μA , and the reaction was left during seven days. Crystals of $[PPh_4][Ni(Me-thiazds)_2]_3$ were collected on the anode as long needles.

$[NEt_4][Ni(Me-thiazds)_2]_2$. A solution of Et_4NBF_4 (200 mg) dissolved in 10 mL of acetone was introduced in both compartments as supporting electrolyte. The nickel complex $[NEt_4][Ni(Me-thiazds)_2]$ (10 mg) was introduced in the anodic compartment. The current intensity was adjusted to 0.5 μA , and the reaction was left during seven days. Crystals of $[NEt_4][Ni(Me-thiazds)_2]_2$ were collected on the anode as long needles.

$[NBu_4]_3[Ni(Me-thiazds)_2]_2$. A solution of Bu_4NPF_6 (200 mg) dissolved in 10 mL of CH_3CN was introduced in both compartments as supporting electrolyte. The nickel complex $[NBu_4][Ni(Me-thiazds)_2]$ (10 mg) was introduced in the anodic compartment. The current intensity was adjusted to 0.5 μA , and the reaction was left during seven days. Crystals of $[NBu_4][Ni(Me-thiazds)_2]_2$ were collected on the anode as long needles.

X-Ray Crystallography. Data collections were performed on an APEXII Bruker-AXS diffractometer equipped with a CCD camera for $[Ni(Me-thiazds)_2]$, on D8 VENTURE Bruker AXS diffractometer for and on XtaLAB AFC11 Rigaku diffractometer for $[Ph_4P][Pt(Me-thiazdt)_2]$. Structures were solved by direct methods using the *SIR97* program,³³ and then refined with full-matrix least-square methods based on F^2 (*SHELXL-97*)³⁴ with the aid of the *WINGX* program.³⁵ All non-hydrogen atoms were refined with anisotropic atomic displacement parameters. H atoms were finally included in their calculated positions. Details of the final refinements are summarized in Table 3.

Table 3. Crystallographic data^{a,b}

	[PPh ₄] [Ni(Me-thiazds) ₂]	[PPh ₄] [Ni(Me-thiazds) ₂] ₃	[Et ₄ N] [Ni(Me-thiazds) ₂] ₂	[nBu ₄ N] _{0.66} [Ni(Me-thiazds) ₂] ₂
CCDC	2224750	2224751	2224748	2224749
Formulae	C ₃₂ H ₂₆ N ₂ NiPS ₄ Se ₄	C ₄₈ H ₃₈ N ₆ Ni ₃ PS ₁₂ Se ₁₂	C ₁₂ H ₁₆ N _{2.5} NiS ₄ Se ₄	C ₈ H ₆ N ₂ NiS ₄ Se ₄
FW (g.mol ⁻¹)	972.31	2238.18	698.06	632.94
System	monoclinic	monoclinic	triclinic	triclinic
Space group	<i>P</i> 2 ₁ / <i>n</i>	<i>C</i> 2/ <i>c</i>	<i>P</i> $\bar{1}$	<i>P</i> $\bar{1}$
a (Å)	10.6095(8)	49.634(5)	6.4328(5)	6.4074(9)
b (Å)	19.6820(14)	7.3788(7)	8.1900(3)	8.1303(11)
c (Å)	16.5774(13)	20.312(2)	18.7194(13)	19.673(3)
α (deg)	90	90	91.113(4)	82.976(5)
β (deg)	99.828(3)	113.440(4)	99.767(6)	89.302(5)
γ (deg)	90	90	91.548(5)	88.260(5)
V (Å ³)	3410.8(4)	6825.2(12)	971.29(11)	1016.6(3)
T (K)	150(2)	150(2)	293(2)	150(2)
Z	4	4	2	2
D _{calc} (g.cm ⁻³)	1.893	2.178	2.387	2.068
μ (mm ⁻¹)	5.157	7.649	8.923	8.513
Total refls	48468	43482	12136	33238
Abs corr	multiscan	multiscan	multiscan	multiscan
Uniq refls (R _{int})	7818(0.0893)	7591 (0.1099)	4561 (0.0463)	4654 (0.0765)
Uniq refls (I > 2σ(I))	6314	6251	3067	3820
R ₁ , wR ₂	0.0575, 0.124	0.0597, 0.1174	0.0669, 0.14	0.0449, 0.1019
R ₁ , wR ₂ (all data)	0.0773, 0.133	0.0786, 0.1225	0.1139, 0.1621	0.0575, 0.1081
GOF	1.109	1.136	1.075	1.025

^aR₁ = $\sum ||F_o| - |F_c|| / \sum |F_o|$. ^bwR₂ = $[\sum (F_o^2 - F_c^2)^2] / [\sum (F_o^2)^2]^{1/2}$.

Transport measurements. Single crystals were mounted in the DAC by using the same technique as reported earlier.³⁶ The sample was encapsulated with a mixture of epoxy and alumina. The diamond culet size was 0.7 mm. Electrical contacts were obtained by attaching four 10 μm gold wires with gold paint, and the four-probe DC method was used for all measurements. The contacts were made on the corners of the elongated plates. The stacking axis of the trimers/dimers in the three mixed-valence salts is located within this plane, as illustrated in Fig. S7 for [nBu₄N]_{0.66}[Ni(Me-thiazds)₂]₂. Daphne Oil 7373 was used as the pressure transmitting medium. The pressure was determined by the shift in the ruby fluorescence R1 lines at room temperature.

Band structure calculations. The first-principles calculations for the solid were carried out using a numeric atomic orbitals density functional theory (DFT) approach^{37,38} developed for efficient calculations in large systems and implemented in the SIESTA code.³⁹ We used the generalized gradient approximation (GGA) to DFT and, in particular, the functional of Perdew, Burke, and Ernzerhof.⁴⁰ To study the relative energies of states with localized electrons, spin polarized band calculations for appropriate supercells have been undertaken. All calculations included a Hubbard correction term $U_{\text{eff}} = 6.0$ eV for the S 3p and Se 4p states.⁴¹ In previous work⁴² we have found that this U term on the chalcogen atoms is needed for appropriately describing the electronic structure of molecular conductors where accurate experimental information on the bandwidth and charge transfer is available. Only the valence electrons are considered in the calculation, with the core being replaced by norm-conserving scalar relativistic pseudopotentials⁴³ factorized in the Kleinman-Bylander form.⁴⁴ We have used a split-valence double- ζ basis set including polarization orbitals with an energy shift of 10 meV for all atoms.⁴⁵ The energy cutoff of the real space integration mesh was 350 Ry. The Brillouin zone was sampled using grids⁴⁶ of $(10 \times 10 \times 5)$ k -points for the calculations using a single cell; those for larger unit cells were modified appropriately. The experimental crystal structures were used for the computations.

The tight-binding band structure calculations were of the extended Hückel type⁴⁷ and used a modified Wolfsberg–Helmholtz formula⁴⁸ to calculate the non-diagonal $H_{\mu\nu}$ values. All valence electrons were considered in the calculations and the basis set consisted of Slater-type orbitals of double- ζ quality for Ni 3d and of single- ζ quality for Ni 3s and 3p, C 2s and 2p, S 3s and 3p, Se 4s and 4p and H 1s. The ionization potentials, contraction coefficients and exponents were taken from previous work.⁴⁹

■ ASSOCIATED CONTENT

Supporting Information

The Supporting Information is available free of charge at <https://pubs.acs.org/doi/10.1021/acs.inorgchem.XXXX>.

Figures S1–S7 (PDF): Additional crystal structure figure, Temperature dependence of the magnetic susceptibility curves, calculated extended Hückel band structure, Calculated DFT band structures, crystal faces indexation.

Accession Codes

CCDC 2224748-2224751 contain the supplementary crystallographic data for this paper. These data can be obtained free of charge via www.ccdc.cam.ac.uk/data_request/cif, or by emailing data_request@ccdc.cam.ac.uk, or by contacting The Cambridge Crystallographic Data Centre, 12 Union Road, Cambridge CB2 1EZ, UK; fax: +44 1223 336033.

■ AUTHOR INFORMATION

Corresponding Authors

Enric Canadell – *Institut de Ciència de Materials de Barcelona, ICMA-B-CSIC, Campus de la UAB, 08193 Bellaterra, Spain*; orcid.org/0000-0002-4663-5226; Email: canadell@icmab.es

Marc Fourmigué – *Institut des Sciences Chimiques de Rennes, Université de Rennes, CNRS, UMR 6226, F-35000 Rennes, France*; orcid.org/0000-0002-3796-4802; Email: marc.fourmigue@univ-rennes1.fr

Dominique Lorcy – *Institut des Sciences Chimiques de Rennes, Université de Rennes, CNRS, UMR 6226, F-35000 Rennes, France*; orcid.org/0000-0002-7698-8452; Email: dominique.lorcy@univ-rennes1.fr

Authors

Hadi Hachem – *Institut des Sciences Chimiques de Rennes, Université de Rennes, CNRS, UMR 6226, F-35000 Rennes, France*

HengBo Cui – *(a) Condensed Molecular Materials Laboratory, RIKEN, Wako-shi, Saitama 351-0198, Japan (b) New address: Department of Physics and Astronomy, Institute of Applied Physics, Seoul National University, Seoul 08826, Korea*

Reizo Kato – *Condensed Molecular Materials Laboratory, RIKEN, Wako-shi, Saitama 351-0198, Japan*; orcid.org/0000-0002-2606-4657

Pere Alemany – *Departament de Ciència de Materials i Química Física and Institut de Química Teòrica i Computacional (IQTCUB), Universitat de Barcelona, Martí i Franquès 1, E-08028 Barcelona, Spain*; orcid.org/0000-0002-3139-6189

Olivier Jeannin – *Institut des Sciences Chimiques de Rennes, Université de Rennes, CNRS, UMR 6226, F-35000 Rennes, France; orcid.org/0000-0002-1411-5656*

Notes

The authors declare no competing financial interest.

■ ACKNOWLEDGMENTS

This work was supported in part by Université de Rennes 1 (PhD grant to H. H.) and by the JSPS KAKENHI (Grant JP16H06346). The stay of H. H. to RIKEN was supported in part by RIKEN International Program Associate and by Rennes Métropole. We thank Takaaki Minamidate (RIKEN) and Thierry Guizouarn (Rennes) for the magnetic susceptibility (SQUID) measurements. Work in Spain was supported by MINECO through Grants PGC2018-096955-B-C44 and PID2021-128217NB-I00, Generalitat de Catalunya (2017SGR1506 and 2017SGR1289). E. C. acknowledges support of the Spanish MINECO through the Severo Ochoa FUNFUTURE (CEX2019-000917-S) Excellence Centre distinction and P. A. from the Maria de Maeztu Units of Excellence Program (MDM-2017-0767). Their support is gratefully acknowledged.

■ REFERENCES

- ¹ (a) Kobayashi, A.; Fujiwara, E.; Kobayashi, H. Single-component molecular metals with extended-TTF dithiolate ligands. *Chem. Rev.* **2004**, *104*, 5243–5264. (b) Garreau-de Bonneval, B.; Moineau-Chane Ching, K. I.; Alary, F.; Bui, T. T.; Valade, L. Neutral d⁸ metal bis-dithiolene complexes: synthesis, electronic properties and applications. *Coord. Chem. Rev.* **2010**, *254*, 1457–1467. (c) Papavassiliou, G. C.; Anyfantis, G. C.; Mousdis, G. A. Neutral metal-1,2-dithiolenes: preparations, properties and possible applications of unsymmetrical in comparison to the symmetrical. *Crystals*, **2012**, *2*, 762–811. (d) Pop, F.; Avarvari, N. Chiral metal-dithiolene complexes. *Coord. Chem. Rev.* **2017**, *346*, 20–31. (e) Naito, T. Prototype Material for New strategy of photon energy storage. *Inorganics*, **2020**, *8*, 53 (1–27). (f) Velho, M. F. G.; Silva, R. A.L.; Belo, D. The quest for single component molecular metals within neutral transition metal complexes. *J. Mater. Chem. C* **2021**, *9*, 10591–10609.
- ² (a) Robertson, N.; Cronin, L. Metal bis-1,2-dithiolene complexes in conducting or magnetic crystalline assemblies. *Coord. Chem. Rev.* **2002**, *227*, 93–127. (b) Canadell, E. Electronic

- structure of transition metal complex-based molecular metals and superconductors. *Coord. Chem. Rev.* **1999**, *185-186*, 629–651. (c) Pullen, A. E.; Olk, R.-M. The coordination chemistry of 1,3-dithiole-2-thione-4,5-dithiolate (dmit) and isologs. *Coord. Chem. Rev.* **1999**, *188*, 211–262. (d) Cassoux, P.; Valade, L.; Kobayashi, H.; Kobayashi, A.; Clark, R. A. Underhill, A. E. Molecular metals and superconductors derived from metal complexes of 1,3-dithiol-2-thione-4,5-dithiolate (dmit). *Coord. Chem. Rev.* **1991**, *110*, 115–160.
- ³ (a) Kato, R. Development of π -Electron Systems Based on $[M(\text{dmit})_2]$ ($M = \text{Ni}$ and Pd ; dmit: 1,3-dithiole-2-thione-4,5-dithiolate) Anion Radicals. *Bull. Chem. Soc. Jpn.* **2014**, *87*, 355–374. (b) Kato, R. Conducting Metal Dithiolene Complexes: structural and electronic Properties. *Chem. Rev.* **2004**, *104*, 5319–5346.
- ⁴ (a) Bowlas, C. J.; Underhill, A. E.; Thetford, D. The synthesis and properties of metal bis-dithiolenes based on the new DMAD ligand. *Synth. Metals*, **1993**, *55-57*, 2158–2163. (b) Best, S. P.; Ciniawsky, S. A.; Clark, R. J. H.; McQueen, R. C. S. Infrared spectroelectrochemical studies of bis(1,2-dithiolene) complexes of transition metals. *J. Chem. Soc. Dalton Trans.* **1993**, 2267–2271. (c) Charlton, A.; Underhill, A. E.; Kobayashi, A.; Kobayashi, H. Syntheses, characterisation and crystal structures of metal complexes of a novel 1,2-dithiolate ligand, 6,7-dihydro-6-methylene-5H-1,4-dithiepine-2,3-dithiol. *J. Chem. Soc., Dalton Trans.* **1995**, 1285–1295. (d) Nakano, M.; Kuroda, A.; Matsubayashi, G.-E. Extended bisdithiolene metal complexes: preparation and electrical conductivities of $[M(\text{C}_8\text{H}_4\text{S}_8)_2]$ anion complexes ($M = \text{Ni(II)}$, Pt(II) , Au(III)). *Inorg. Chim. Acta*, **1997**, *254*, 189–193. (e) Cleary, C. F.; Robertson, N.; Takahashi, M.; Underhill, A. E.; Hibbs, D. E.; Hursthouse, M. B.; Malik, K. M. A. Synthesis and characterization of $[\text{PPh}_4][\text{M}(\text{diod})_2]$, $M = \text{Ni}$, Pd , Cu or Au ; crystal structure of $[\text{PPh}_4][\text{Cu}(\text{diod})_2]$. *Polyhedron*, **1997**, *16*, 1111–1117. (f) Takahashi, M.; Robertson, N.; Kobayashi, A.; Becker, H.; Friend, R. H.; Underhill, A. E. Synthesis, structure and properties of new dithiolene complexes containing a 1,3,5-trithiepin ring. *J. Mater. Chem.* **1998**, *8*, 319–324.
- ⁵ (a) Dautel, O. J., Fourmigué, M., Canadell, E.; Auban-Senzier, P. Fluorine segregation controls the solid-state organization and electronic properties of Ni and Au dithiolene complexes: stabilization of a conducting single-component gold dithiolene complex. *Adv. Funct. Mater.* **2002**, *12*, 693–698. (b) Jeannin, O.; Fourmigué, M. Perylene salts of unsymmetrical nickel and gold dithiolene complexes with 3:2 stoichiometry: conformational polymorphism and strong antiferromagnetic interactions. *New J. Chem.* **2006**, *30*, 1774–1781. (c) Jeannin, O.; Fourmigué, M. BEDT-TTF salts of the unsymmetrical $[\text{M}(\text{tfadt})_2]^-$ dithiolene complexes ($M = \text{Ni}$, Au ; $\text{tfadt} = \text{S}_2\text{C}_2(\text{CN})(\text{CF}_3)$). *Inorg. Chim. Acta*, **2007**, *360*, 3820–3824.

- (d) Ray, K.; George, S. D.; Solomon, E. I.; Wieghardt, K.; Neese, F. Description of the Ground-State Covalencies of the Bis(dithiolato) Transition-Metal Complexes from X-ray Absorption Spectroscopy and Time-Dependent Density-Functional Calculations. *Chem. Eur. J.* **2007**, *13*, 2783–2797. (e) Skabara, P. J.; Pozo-Gonzalo, C.; Miazza, N. L.; Laguna, M.; Cerrada, E.; Luquin, A.; Gonzalez, B.; Coles, S. J.; Hursthouse, M. B.; Harrington R. W.; Clegg, W. Novel dithiolene complexes incorporating conjugated electroactive ligands. *Dalton Trans.* **2008**, 3070–3079.
- ⁶ (a) Perochon, R. Piekara-Sady, L.; Jurga, W.; Clérac, R.; Fourmigué, M. Amphiphilic paramagnetic neutral gold dithiolene complexes. *Dalton Trans.* **2009**, 3052–3061. (b) Rabaça, S.; Cerdeira, A. C.; Neves, A. I. S.; Dias, S. I. G.; Mézière, C.; Santos, I. C.; Pereira, L. C. J.; Fourmigué, M.; Henriques, R. T.; Almeida, M. Complexes based on asymmetrically substituted pyridine-dithiolene ligands [M(4-pedt)₂] (M = Au, Cu, Ni; 4-pedt = 1-(pyridin-4-yl)-ethylene-1,2-dithiolate): Synthesis, structure and physical properties. *Polyhedron*, **2009**, *28*, 1069–1078. (c) Perochon, R.; Poriel, C.; Jeannin, O.; Piekara-Sady, L.; Fourmigué, M. Chiral, Neutral, and Paramagnetic Gold Dithiolene Complexes Derived from Camphorquinone. *Eur. J. Inorg. Chem.* **2009**, 5413–5421. (d) Brooks, A. C.; Day, P.; Dias, S. I. G.; Rabaça, S.; Santos, I. C.; Henriques, R. T.; Wallis, J. D.; Almeida, M. Pyridine-functionalised (vinylenedithio)tetrathiafulvalene (VDT-TTF) derivatives and their dithiolene analogues. *Eur. J. Inorg. Chem.* **2009**, 3084–3093.
- ⁷ (a) Nomura, M.; Harada, K.; Suzuki, T.; Kajitani, M.; Sugiyama, T. Square-planar metal dithiolene complexes (M = Ni, Au) exhibiting *cis* and *trans* forms based on structurally flexible *o*-xylylene backbone. *Polyhedron*, **2012**, *47*, 9–15. (b) Rabaça, S.; Cerdeira, A. C.; Oliveira, S.; Santos, I. C.; Henriques, R. T.; Pereira, L. C. J.; Coutinho, J. T.; Almeida, M. Neutral gold and nickel bis[1-(pyridin-4-yl)-ethylene-1,2-dithiolene] complexes: Synthesis, structure and physical properties. *Polyhedron*, **2012**, *39*, 91–98. (c) Cerdeira, A. C.; Afonso, M. L.; Santos, I. C.; Pereira, L. C. J.; Coutinho, J. T.; Rabaça, S.; Simao, D.; Henriques, R. T.; Almeida, M. Synthesis, structure and physical properties of transition metal bis 4-cyanobenzene-1,2-dithiolate complexes [M(cbdt)₂]^{z-} (M = Zn, Co, Cu, Au, Ni, Pd, z = 0, 1, 2). *Polyhedron* **2012**, *44*, 228–237. (d) Hu, L.; Qin, J.; Zhou, N.; Meng, Y.-F.; Xu, Y.; Zuo, J.-L.; You, X.-Z. Synthesis, characterization, and optical properties of new metal complexes with the multi-sulfur 1,2-dithiolene ligand. *Dyes and Pigments*, **2012**, *92*, 1223–1230.
- ⁸ (a) Neves, A. I. S.; Santos, I. C.; Coutinho, J. T.; Pereira, L. C. J.; Henriques, R. T.; Lopes, E. B.; Alves, A.; Almeida, M.; Belo, D. 5-Methylthiophene-2,3-dithiolene Transition Metal

- Complexes. *Eur. J. Inorg. Chem.* **2014**, 3989–3999. (b) Mebrouk, K.; Kaddour, W.; Auban-Senzier, P.; Pasquier, C.; Jeannin, O.; Camerel, F.; Fourmigué, M. Molecular Alloys of Neutral Gold/Nickel Dithiolene Complexes in Single-Component Semiconductors, *Inorg. Chem.* **2015**, *54*, 7454–7460. (c) Branzea, D. G.; Pop, F.; Auban-Senzier, P.; Clérac, R.; Alemany, P.; Canadell, E.; Avarvari, N. Localization versus delocalization in chiral single component conductors of gold bis(dithiolene) complexes. *J. Am. Chem. Soc.* **2016**, *138*, 6838–6851. (d) Andrade, M. M.; Silva, R. A. L.; Santos, I. C.; Lopes, E. B.; Rabaça, S.; Pereira, L. C. J.; Coutinho, J. T.; Telo, J. P.; Rovira, C.; Almeida, M.; Belo, D. Gold and nickel alkyl substituted bis-thiophenedithiolene complexes: anionic and neutral forms. *Inorg. Chem. Front.*, **2017**, *4*, 270–280. (e) Hachem, H.; Jeannin, O.; Fourmigué, M.; Barrière, F.; Lorcy, D. Halogen bonded metal bis(dithiolene) 2D frameworks. *CrystEngComm*, **2020**, *22*, 3579–3587. (f) Hachem, H.; Bellec, N.; Fourmigué, M.; Lorcy, D. Hydrogen bonding interactions in single component molecular conductors based on metal (Ni, Au) bis(dithiolene) complexes. *Dalton Trans*, **2020**, *49*, 6056–6064.
- ⁹ Eid, S.; Fourmigué, M.; Roisnel, T.; Lorcy, D. Influence of the thiazole backbone on the structural, redox, and optical properties of dithiolene and diselenolene complexes. *Inorg. Chem.* **2007**, *46*, 10647–10654.
- ¹⁰ (a) Filatre-Furcate, A.; Bellec, N.; Jeannin, O.; Auban-Senzier, P.; Fourmigué, M.; Vacher, A.; Lorcy, D. Radical or not radical: compared structures of metal (M = Ni, Au) bis-dithiolene complexes with a thiazole backbone. *Inorg. Chem.*, **2014**, *53*, 8681–8690. (b) Filatre-Furcate, A.; Roisnel, T.; Le Gal, Y.; Jeannin, O.; Dorcet, V.; Lorcy, D. Comparative structural studies of Ni vs. Au metal bis(dithiolene) complexes with a thiazole backbone [M(R-thiazdt)₂]. *Eur. J. Inorg. Chem.* **2022**, e202200355 (1-9).
- ¹¹ Hachem, H.; Cui, H.; Tsumuraya, T.; Kato, R.; Jeannin, O.; Fourmigué, M.; Lorcy, D. Single component conductors based on closed-shell Ni and Pt bis(dithiolene) complexes: metallization under high pressure. *J. Mater. Chem. C.* **2020**, *8*, 11581–11592.
- ¹² Tenn, N.; Bellec, N.; Jeannin, O.; Piekara-Sady, L.; Auban-Senzier, P.; Íñiguez, J.; Canadell, E.; Lorcy, D. A single-component molecular metal based on a thiazole dithiolate gold complex. *J. Am. Chem. Soc.* **2009**, *131*, 16961–16967.
- ¹³ Le Gal, Y.; Roisnel, T.; Auban-Senzier, P.; Bellec, N.; Íñiguez, J.; Canadell, E.; Lorcy, D. Stable metallic state of a neutral radical single-component conductor at ambient pressure *J. Am. Chem. Soc.*, **2018**, *140*, 6998–7004.
- ¹⁴ (a) Rabaca, S.; Santos, I. C.; Duarte, M. T.; Gama, V. Crystal structure and magnetic behavior of decamethylferrocenium bis(2-thioxo-1,3-dithiole-4,5-diselenolato)nickelate(III). *Inorg.*

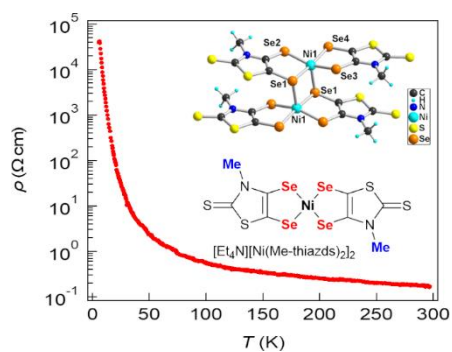
- Chim. Acta* **2007**, *360*, 3855–3860. (b) Cornelissen, J. P.; Haasnoot, J. G.; Reedijk, J.; Faulmann, C.; Legros, J.-P.; Cassoux, P.; Nigrey, P.J. Crystal structures and electrochemical properties of two phases of tetrabutylammonium bis(1,3-dithiole-2-thione-4,5-diselenolato) nickelate(III). *Inorg. Chim. Acta* **1992**, *202*, 131–139.
- ¹⁵ Faulmann, C.; Legros, J.-P.; Cassoux, P.; Cornelissen, J.; Brossard, L.; Inokuchi, M.; Tajima, H.; Tokumoto, M. Synthesis, crystal structure and electrical properties of two new palladium complexes of selenium and sulfur ligands: $[\text{NMe}_4][\text{Pd}(\text{C}_3\text{S}_3\text{Se}_2)_2]_2$ and $[\text{PMe}_4][\text{Pd}(\text{C}_3\text{S}_5)_2]_2$. *J. Chem. Soc., Dalton Trans.* **1994**, 249–254.
- ¹⁶ Olk, R.-M.; Olk, B.; Rohloff, J.; Reinhold, J.; Sieler, J.; Trubenbach, K.; Kirmse, R.; Hoyer, E. Zur Koordinationschemie des 1,3-Dithiol-2-selen-4,5-diselenolats (dsise) und des 1,3-Dithiol-2-selen-4,5-dithiolats (dmise). Kristall- und Molekülstruktur des Tetrabutylammonium bis-(1,3-dithiol-2-selen-4,5-diselenolato)nickelat(II) und -(III), $[(n\text{-C}_4\text{H}_9)_4\text{N}]_2[\text{Ni}(\text{dsise})_2]$ und $(n\text{-C}_4\text{H}_9)_4\text{N}[\text{Ni}(\text{dsise})_2]$. *Z. Anorg. Allg. Chem.* **1992**, *609*, 103–116.
- ¹⁷ Olk, R.-M.; Kirmse, R.; Hoyer, E.; Faulmann, C.; Cassoux, P. Synthese und Eigenschaften von molekularen Leitern auf der Basis von dmit-isologen Chelaten Kristall- und Molekülstruktur des Tetramethylammonium-bis-[bis-(1,3-dithiol-2-selen-4,5 diselenolato)nickelat]: $[(\text{CH}_3)_4\text{N}][\text{Ni}(\text{dsise})_2]_2$. *Z. Anorg. Allg. Chem.* **1994**, *620*, 90–100.
- ¹⁸ Hachem, H.; Cui, H.; Kato, R.; Jeannin, O.; Barrière, F.; Fourmigué, M.; Lorcy, D. Introducing Selenium in Single-Component Molecular Conductors Based on Nickel Bis(dithiolene) Complexes. *Inorg. Chem.* **2021**, *60*, 7876–7886.
- ¹⁹ Yzambart, G.; Bellec, N.; Nasser, G.; Jeannin, O.; Roisnel, T.; Fourmigué, M.; Auban-Senzier, P.; Íñiguez, J.; Canadell, E.; Lorcy, D. Anisotropic chemical pressure effects in single-component molecular metals based on radical dithiolene and diselenolene gold complexes. *J. Am. Chem. Soc.*, **2012**, *134*, 17138–17148.
- ²⁰ Le Gal Y.; Cui, H.; Alemany, P.; Canadell, E.; Kato, R.; Roisnel, T.; Dorcet, V.; Fourmigué, M.; Lorcy, D. Mixed-valence gold bis(diselenolene) complex turning metallic under pressure. *J. Mater. Chem. C.* **2021**, *9*, 12291–12302.
- ²¹ Dithiolene Chemistry, *Prog. Inorg. Chem.* E.I. Stiefel Ed. **2004**, vol. 52
- ²² Kini, A. M.; Beno, M. A.; Budz, S.; Wang, H. H.; Williams, J. M. New Electrically Conducting Solids based on Nickel (II) - Bis(1,3-Dithiole-2-Thione-4,5-Diselenolate). *Mat. Res. Soc. Symp. Proc.* **1990**, *173*, 177–188 (<https://link.springer.com/article/10.1557/PROC-173-177>)

- ²³ Nagapetian, S. S.; Shklover, V. E.; Struchkov, Y. T.; Kotov, A. I.; Yagubskii, E. B.; Ukhin, L. Y. Synthesis and the x-ray study of $[\text{Ni}(\text{dddt})_2]_3(\text{ClO}_4)_2$ – Trimeric cationic dithiolate complex – A precursor of low-dimensional metals of a new type. *Dokl. Akad. Nauk SSSR*, **1990**, *310*, 94–98.
- ²⁴ Canadell, E.; Rachidi, I. E.-I.; Ravy, S.; Pouget, J. P.; Brossard, L.; Legros, J.-P. On the band electronic structure of $\text{X}[\text{M}(\text{dmit})_2]_2$ ($\text{X} = \text{TTF}, (\text{CH}_3)_4\text{N}$; $\text{M} = \text{Ni}, \text{Pd}$) molecular conductors and superconductors. *J. Phys. (Paris)* **1989**, *50*, 2967–2981.
- ²⁵ Alemany, P.; Pouget, J.-P.; Canadell, E. Structural and electronic control of the metal to insulator transition and local orderings in the theta- $(\text{BEDT-TTF})_2\text{X}$ organic conductors *J. Phys: Condens. Matter* **2015**, *27*, 465702.
- ²⁶ Abhervé, A.; Mroweh, N.; Cauchy, T.; Pop, F.; Cui, H.; Kato, R.; Vanthuyne, N.; Alemany, P.; Canadell, E.; Avarvari, N. Conducting chiral nickel(II) bis(dithiolene) complexes: structural and electron transport modulation with the charge and the number of stereogenic centres. *J. Mater. Chem. C*, **2021**, *9*, 4119–4140.
- ²⁷ Canadell, E.; Ravy, S.; Pouget, J. P.; Brossard, L. Concerning the Band Structure of $\text{D}[\text{M}(\text{dmit})_2]_2$ ($\text{D} = \text{TTF}, \text{Cs}, \text{NMe}_4$; $\text{M} = \text{Ni}, \text{Pd}$) Molecular Conductors and Superconductors: Role of the HOMO and LUMO. *Solid State Comm.* **1990**, *75*, 633–638.
- ²⁸ Alemany, P.; Pouget, J.-P.; Canadell, E. Electronic structure and anion ordering in $(\text{TMTSF})_2\text{ClO}_4$ and $(\text{TMTSF})_2\text{NO}_3$: A first-principles study. *Phys. Rev. B* **2014**, *27*, 155124
- ²⁹ Mott, N. F. *Metal-Insulator Transitions*; Barnes and Noble: New York, 1977.
- ³⁰ Anderson, P. W. Absence of Diffusion in Certain Random Lattices. *Phys. Rev.* **1968**, *109*, 1492–1505.
- ³¹ Hayes, W.; Stoneham, A. M. *Defects and Defect Processes in Non-metallic Solids*, Wiley, New York, 1985; Chapter 8.
- ³² (a) Yamashita, M.; Nakata, N.; Senshu, Y.; Nagata, M.; Yamamoto, H. M.; Kato, R.; Shibauchi, T.; Matsuda, Y. Highly Mobile Gapless Excitations in a Two-Dimensional Candidate Quantum Spin Liquid. *Science* **2010**, *328*, 1246–1248. (b) Itou, T.; Oyamada, A.; Maegawa, S.; Kato, R. Instability of a quantum spin liquid in an organic triangular-lattice antiferromagnet. *Nature Phys.* **2010**, *6*, 673–676. (c) Yamashita, S.; Yamamoto, T.; Nakazawa, Y.; Tamura, M.; Kato, R. Gapless spin liquid of an organic triangular compound evidenced by thermodynamic measurements. *Nature Commun.* **2011**, *2*, 275.
- ³³ Altomare, A.; Burla, M. C.; Camalli, M.; Cascarano, G.; Giacovazzo, C.; Guagliardi, A.; Moliterni, A. G. G.; Polidori, G.; Spagna, R. SIR97: a new tool for crystal structure determination and refinement. *J. Appl. Cryst.* **1999**, *32*, 115–119.

- ³⁴ Sheldrick, G. M. A short history of SHELX. *Acta Crystallogr.* **2008**, *A64*, 112–122.
- ³⁵ Farrugia, L. J. WinGX and ORTEP for Windows: an update. *J. Appl. Cryst.* **2012**, *45*, 849–854.
- ³⁶ Cui, H.; Brooks, J. S.; Kobayashi, A.; Kobayashi, H. Metallization of the Single Component Molecular Semiconductor [Ni(ptdt)₂] under Very High Pressure. *J. Am. Chem. Soc.* **2009**, *131*, 6358–6359.
- ³⁷ Hohenberg, P.; Kohn, W. Inhomogeneous Electron Gas. *Phys. Rev.* **1964**, *136*, B864–871.
- ³⁸ Kohn, W.; Sham, L. J. Self-Consistent Equations Including Exchange and Correlation Effects. *Phys. Rev.* **1965**, *140*, A1133–1138.
- ³⁹ (a) Soler, J. M.; Artacho, E.; Gale, J. D.; García, A.; Junquera, J.; Ordejón, P.; Sánchez-Portal, D. The Siesta method for ab initio order-N materials simulation. *J. Phys.: Condens. Matter.* **2002**, *14*, 2745–2779. (b) Artacho, E.; Anglada, E.; Diéguez, O.; Gale, J. D.; García, A.; Junquera, J.; Martín, R. M.; Ordejón, P.; Pruneda, J. M.; Sánchez-Portal, D.; Soler, J. M. The Siesta method; developments and applicability. *J. Phys.: Condens. Matter.* **2008**, *20*, 064208. (c) García, A.; Papior, N.; Akhtar, A.; Artacho, E.; Blum, V.; Bosoni, E.; Brandimarte, P.; Brandbyge, M.; Cerdá, J. I.; Corsetti, F.; Cuadrado, R.; Dikan, V.; Ferrer, J.; Gale, J. D.; García-Fernández, P.; García-Suárez, V. M.; García, S.; Huhs, G.; Illera, S.; Korytar, R.; Koval, P.; Lebedeva, I.; Lin, L.; López-Tarifa, P.; Mayo, S. G.; Mohr, S.; Ordejón, P.; Postnikov, A.; Pouillon, Y.; Pruneda, M. A.; Robles, R.; Sánchez-Portal, D.; Soler, J. M.; Ullah, R.; Yu, V. W.; Junquera, J. Siesta: Recent developments and applications. *J. Chem. Phys.* **2020**, *152*, 204108. (d) For more information on the SIESTA code visit: <http://departments.icmab.es/leem/siesta/>.
- ⁴⁰ Perdew, J. P.; Burke, K.; Ernzerhof, M. Generalized Gradient Approximation Made Simple. *Phys. Rev. Lett.* **1996**, *77*, 3865–3868.
- ⁴¹ Dudarev, S. L.; Botton, G. A.; Savrasov, S. Y.; Humphreys, C. J.; Sutton, A. P. Electron-energy-loss spectra and the structural stability of nickel oxide: An LSDA+U study. *Phys. Rev. B* **1998**, *57*, 1505–1509.
- ⁴² Kiyota, Y.; Jeon, I.-R.; Jeannin, O.; Beau, M.; Kawamoto, T.; Alemany, P.; Canadell, E.; Mori, T.; Fourmigué, M. Electronic engineering of a tetrathiafulvalene charge-transfer salt via reduced symmetry induced by combined substituents. *Phys. Chem. Chem. Phys.*, **2019**, *21*, 22639–22646.
- ⁴³ Troullier, N.; Martins, J. L. Efficient pseudopotentials for plane-wave calculations. *Phys. Rev. B* **1991**, *43*, 1993–2006.

- ⁴⁴ Kleinman, L.; Bylander, D. M. Efficacious Form for Model Pseudopotentials. *Phys. Rev. Lett.* **1982**, *48*, 1425–1428.
- ⁴⁵ Artacho, E.; Sánchez-Portal, D.; Ordejón, P.; García, A.; Soler, J. M. Linear-Scaling ab-initio Calculations for Large and Complex Systems. *Physica Status Solidi (b)* **1999**, *215*, 809–817.
- ⁴⁶ Monkhorst, H. J.; Pack, J. D. Special points for Brillouin-zone integrations. *Phys. Rev. B* **1976**, *13*, 5188–5192.
- ⁴⁷ Whangbo, M.-H.; Hoffmann, R. The Band Structure of the Tetracyanoplatinate Chain. *J. Am. Chem. Soc.* **1978**, *100*, 6093–6098.
- ⁴⁸ Ammeter, J. H.; Bürgi, H.-B.; Thibeault, J.; Hoffmann, R. Counterintuitive Orbital Mixing in Semiempirical and ab Initio Molecular Orbital Calculations. *J. Am. Chem. Soc.* **1978**, *100*, 3686–3692
- ⁴⁹ Curreli, S.; Deplano, P.; Mercuri, M. L.; Pilia, L. Serpe, A.; Bigoli, F.; Pellinghelli, M. A.; Coronado, E.; Gómez-García, C. J.; Canadell, E. A New Conducting Molecular Solid Based on the Magnetic $[\text{Ni}(\text{dmf})_6]^{2+}$ Cation and on $[\text{Ni}(\text{dsit})_2]_2^{2-}$ (dsit=1,3-dithiole-2-thione-4,5-diselenolate) Showing an Unprecedented Anion Packing. *J. Solid. State Chem.* **2002**, *168*, 653-660.

For Table of content only



Synopsis

Dimeric or trimeric associations are observed in highly conducting mixed-valence nickel bis(diselenolene) complexes, depending on the nature of the counter ion (Ph_4P^+ , Et_4N^+ , Bu_4N^+) and the stoichiometry of the salt